Numerical simulation of biofilm accumulation in pipelines
by Sandor Szego

A thesis submitted in partial fulfillment of the requirements for the degree of Master of Science in Computer Science
Montana State University
© Copyright by Sandor Szego (1992)

Abstract:
Biofilms can be found in many natural and industrial systems. Their effects can be beneficial or damaging, therefore a need to control these complex ecological systems emerges. This thesis describes a computer model for biofilm accumulation in pipeline systems. First, from an initial conceptual model a mathematical model is derived using the conservation of mass principle. The resulting equations are non-linear, coupled, partial differential equations. A numerical method, using a finite volume approach, is developed to solve the system of equations in time and space. Since the geometry of the system changes due to biofilm accumulation, the grid must adjust itself to the changing geometry. A general three-point integration formula is used to advance the solution in time. Since the formula is nonlinear in the unknowns, Newton's Method is used to solve the discretized equations at every time step. Initial experiments and results are described to show the validity of the developed computer model. The behavior of the model is analyzed as selected numeric parameters are varied. The results are promising, though future work has to determine the predictive capacity of the model by comparing its output to real measurements.

NUMERICAL SIMULATION OF BIOFILM ACCUMULATION IN PIPELINES

by

Sandor Szego

A thesis submitted in partial fulfillment
of the requirements for the degree

of

Master of Science

in

Computer Science

MONTANA STATE UNIVERSITY
Bozeman, Montana

July 1992

N378
Sz24

APPROVAL

of a thesis submitted by

Sandor Szego

This thesis has been read by each member of the thesis committee and has been found to be satisfactory regarding content, English usage, format, citations, bibliographic style and consistency and is ready for submission to the College of Graduate Studies.

July 8, 1992
Date

J. Dubrigh Stanley
Chairperson, Graduate Committee

Approved for the Major Department

July 8, 1992
Date

J. Dubrigh Stanley
Head, Major Department

Approved for the College of Graduate Studies

July 10, 1992
Date

R. L. Brown
Graduate Dean

STATEMENT OF PERMISSION TO USE

In presenting this thesis in partial fulfillment of the requirements for a master's degree at Montana State University, I agree that the Library shall make it available to borrowers under rules of the Library. Brief quotations from this thesis are allowable without special permission, provided that accurate acknowledgement of source is made.

Permission for extensive quotation from or reproduction of this thesis may be granted by my major professor, or in his/her absence, by the Dean of Libraries when, in the opinion of either, the proposed use of the material is for scholarly purposes. Any copying or use of the material in this thesis for financial gain shall not be allowed without my written permission.

Signature Sarah Lego

Date July 8, 1992

TABLE OF CONTENTS

TABLE OF CONTENTS - Continued

LIST OF TABLES

LIST OF FIGURES

LIST OF FIGURES - Continued

ABSTRACT

Biofilms can be found in many natural and industrial systems. Their effects can be beneficial or damaging, therefore a need to control these complex ecological systems emerges. This thesis describes a computer model for biofilm accumulation in pipeline systems. First, from an initial conceptual model a mathematical model is derived using the conservation of mass principle. The resulting equations are non-linear, coupled, partial differential equations. A numerical method, using a finite volume approach, is developed to solve the system of equations in time and space. Since the geometry of the system changes due to biofilm accumulation, the grid must adjust itself to the changing geometry. A general three-point integration formula is used to advance the solution in time. Since the formula is nonlinear in the unknowns, Newton's Method is used to solve the discretized equations at every time step. Initial experiments and results are described to show the validity of the developed computer model. The behavior of the model is analyzed as selected numeric parameters are varied. The results are promising, though future work has to determine the predictive capacity of the model by comparing its output to real measurements.

CHAPTER 1

INTRODUCTION

This thesis describes a computer model for biofilm processes in a pipeline. A *biofilm* is a layer of fixed biomass composed of microbial organisms and organic polymers of microbial origin attached to a solid surface (substratum). In the vernacular, a biofilm might be called slime or sludge. Simple — typically laboratory developed — biofilms consist of a single species, while naturally occurring biofilms can contain a number of different microorganisms. These species are subject to different interactions, such as symbiosis, competition for common substrates, etc. A very important characteristic of these complex ecological systems is that they can have a significant impact on the surrounding environment, e.g., by introducing corrosion on a metal surface. Biofilms occur in nature without human interaction, or can artificially be introduced to industrial or natural systems. Table 1 gives a few examples of systems where biofilms can and do exist, and also lists some of their effects. These examples show that some biofilms can serve beneficial purposes, while others can cause extensive damage in the natural or industrial environment. Understanding the processes and interactions occurring in these systems, and formulating conceptual and mathematical models enable us to control biofilm processes, and thus reduce their negative

and enhance their positive effects.

A detailed conceptual description of biofilms is required in order to be able to come up with a suitable mathematical model. It is important to distinguish between biofilms and biofilm systems. A biofilm system consists of five compartments [3]:

- Substratum. The solid surface where the microorganisms attach.
- Base film. Structured accumulation of cells.
- Surface film. Provides the transition between the base film and the bulk compartment.
- Bulk liquid. The flow regime of this compartment determines mass and heat transfer between the liquid and the film.
- Gas. Provides aeration or removal of gaseous reaction products.

The biofilm is the combination of the base film and the surface film. A very important characteristic of a biofilm is that a certain (typically large) portion of its volume consists of the continuous liquid medium (liquid phase). For example, in Characklis et al. [5] the data reported suggests that their *Pseudomonas Aeruginosa* biofilm was $\approx 90\%$ water.

Components of biofilm systems are cells, organic and inorganic products, substrates (growth limiting nutrients), and other nutrients. *Interactions* and *processes* between

Process	Effects
Biofilm in heat exchangers	Increased heat transfer resistance
Biofilm in porous media (soil)	Increased fluid resistance
Corrosion due to microbial processes	Reduced equipment lifetime
Biofilm in water distribution systems	Health risks
Biofilm on teeth and gums	Health risk (cavities)
Extraction of toxics from water	Reduced pollutant load

Table 1: Effects of biofilm processes in different systems

these components are transport (advection, diffusion), transfer (cell attachment and detachment, interfacial diffusion), and transformation (chemical reactions).

Geometric configuration is another very important characteristic of a given system. Two widely studied geometries are Continuous Flow Stirred Tank Reactors (CFSTR) and Plug Flow Reactors (PFR). CFSTRs are well mixed tanks where a continuous flow of reactants is present, and the well mixed bulk is constantly removed to sustain a constant bulk volume. Constituent concentrations in the bulk are constant throughout the CFSTR. PFRs are idealized models of pipelines, where the reactants enter the pipe at the inlet, and products leave the pipe at the outlet. Constituent concentrations can vary from inlet to outlet in the PFR.

Previous mathematical models for multispecies biofilms in CFSTR geometries [10], [4] have been based on the conservation of mass principle. Apart from geometry specific assumptions, many conceptual and mathematical formulations for CFSTR systems can be applied to PFR systems.

Models for biofilm processes can serve a variety of purposes. The purpose could

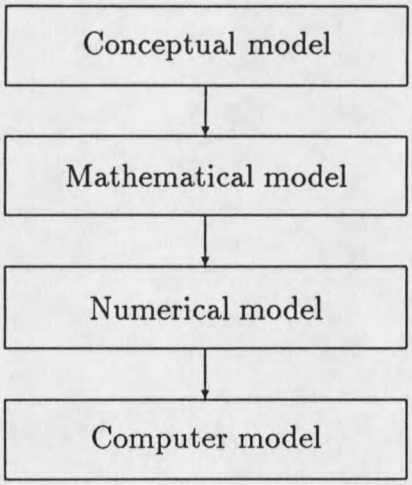

Figure 1: The modeling process

be to predict the concentrations of certain components, or thickness of the formed biofilm. Besides prediction, these models can be used to describe experimental results and to explain the modelers' conceptual understanding of the process . Simulation programs, such as BIOSIM [10], make use of a set of computational units. Each unit is essentially a CFSTR. Two units can be connected in series to simulate other geometries, such as a pipeline.

Previous work on pipelines focused on determining the growth of biofilm on pipewalls and its effect on heat resistance [2]. That model assumes a uniform film consisting of a single species only. It is also assumed that only a single reaction is present in the system and its rate can be expressed using Monod kinetics (to be discussed later).

The goal of this thesis is to describe a computer model for biofilm accumulation in pipelines. The organization follows the basic steps of modeling shown in Figure 1.

In Chapter 2 I give a detailed overview and mathematical formulation of biofilm processes in pipelines. Chapter 3 contains the governing equations that are based on the conservation of mass principle. Chapter 4 explains the numerical methods applied to solve the coupled, non-linear, partial differential equations resulting from the governing equations. Finally, Chapter 5 presents computer simulation runs of different systems.

CHAPTER 2

BIOFILM PROCESSES IN PIPELINES

Many industrial and natural biofilm system geometries can efficiently be modeled by the plug flow reactor. Examples, among many others, include natural streams, heat exchangers, oil pipes, water distribution and waste water systems. A common characteristic of these systems is that there exists a significant advective motion of the liquid medium (bulk compartment) that carries all reactants and products to downstream locations. In fact, this and the existence of radial concentration gradients in the bulk compartment are the only differences between biofilm systems in PFRs and in CFSTRs.

Components

The systems of our concern typically contain the following components: substrates (and nutrients), cells, particles, abiotic components, products, and biocides. For modeling purposes, these components can be divided into two classes:

- Soluble components, and

- Particulate components[1].

In the bulk compartment both classes of components can be described by their concentrations (units: ML^{-3}). The liquid phase in the biofilm compartment could contain all the above components, but the following simplifying assumption is made: *The liquid phase in the film compartment does not contain any particulate components.* There are many ways the concentration (or the mass) of particulates in the film can be defined: (1) X' biofilm particulate mass per unit substratum area (units: ML^{-2}); (2) X biofilm particulate mass per unit biofilm volume (units: ML^{-3}); (3) X'' biofilm particulate mass per unit reactor volume (units: ML^{-3}). Most laboratory measurement methods determine the mass of the particulates in the film using one of the above units. However, it is easy to convert between these units using the relationship $X(\mathbf{x},t) = X'(\mathbf{x},t)/L_F(\mathbf{x},t)$, where $L_F(\mathbf{x},t)$ is the thickness of the film at location $\mathbf{x} = [x,y,z]^T$ and time t. Note that $L_F(\mathbf{x},t)$ is defined as the distance between the surface of the substratum and the surface of the film-liquid interface at point $\mathbf{x}$. Since $\mathbf{x}$ has to lie on the surface of the substratum, it has to satisfy

$$g(\mathbf{x}) = 0, \tag{1}$$

where $g(\cdot)$ defines the surface of the substratum.

In our approach we make use of the second measure, which can be written as

$$X_i = \varepsilon_i(\mathbf{x},t)\varrho_i(\mathbf{x},t), \tag{2}$$

[1]cells and certain products (extracellular polymers)

where X_i is the "concentration" of the *ith* particulate component in the film, ε_i is the fraction of biofilm volume occupied by the *ith* component (void fraction), and ϱ_i is the specific gravity or density of the same component. In general both ε and ϱ can be functions of time t and spatial position $\mathbf{x}$. If we assume that the density of a particulate component is constant (regardless of its position in the film), then (2) becomes

$$X_i(\mathbf{x}, t) = \varepsilon_i(\mathbf{x}, t)\varrho_i. \tag{3}$$

In other words, *if the density (specific gravity) of particulate component i is a known constant*, then by determining $\varepsilon_i(\mathbf{x}, t)$ the concentration of particulate i in the film can be calculated.

The unknown material concentrations can be described as a vector:

$$\mathbf{Q} = \begin{pmatrix} \mathbf{Q_s} \\ \hline \\ \mathbf{Q_p} \end{pmatrix} \tag{4}$$

where the elements of $\mathbf{Q}$ are as follows.

In the bulk,

$$\mathbf{Q_s} = [Q_{si}] = \varepsilon_l C_i,\ i = 1, 2, .., N_{sub} \text{ and} \tag{5}$$

$$\mathbf{Q_p} = [Q_{pi}] = \varepsilon_l C_i,\ i = 1, 2, .., N_{part}, \tag{6}$$

where $\varepsilon_l = 1$ and C_i is the concentration of component i.

In the film,

$$\mathbf{Q_s} = [Q_{si}] = \varepsilon_l C_i,\ i = 1, 2, .., N_{sub} \text{ and} \tag{7}$$

$$\mathbf{Q_p} = [Q_{pi}] = \varepsilon_i \varrho_i,\ i = 1, 2, .., N_{part} - 1, \tag{8}$$

where ε_l is the liquid volume fraction of the biofilm. Note that $\sum_{i=1}^{N_{part}} \varepsilon_i + \varepsilon_l = 1$, thus only $N_{part} - 1$ particulate void fractions (ε_i) are free parameters.

Reactions

The components described in the previous section interact with each other via biochemical reactions. These reactions can be described by their stoichiometric and kinetic coefficients. The stoichiometric equations describe the material balance of a certain reaction, while the kinetic equations determine the rate of the reaction.

The Stoichiometry Matrix

In biofilm systems many biochemical reactions can occur at the same time, such as "growth" reactions for each microorganism and reactions among chemicals (oxidization, reduction). Many components can and do participate in every reaction, thus the stoichiometric equation for the ith reaction has the following form:

$$\alpha_{i,1} P_1 + ... + \alpha_{i,k} P_k \rightarrow \alpha_{i,k+1} P_{k+1} + ... + \alpha_{i,l} P_l. \tag{9}$$

Components on the left hand side of the arrow are consumed and components on the right hand side are produced. If the left hand side coefficients are negated, then the conservation of mass principle leads to

$$\alpha_{i,1} M_{P_1} + ... + \alpha_{i,k} M_{P_k} + \alpha_{i,k+1} M_{P_{k+1}} + ... + \alpha_{i,l} M_{P_l} = 0, \tag{10}$$

where M_{P_i} is the molar weight of component P_i. If the above equation is written for all reactions, then the following matrix equation can be obtained:

$$\boldsymbol{\alpha}\mathbf{M} = 0 \tag{11}$$

where $\boldsymbol{\alpha}$ is the stoichiometry matrix, and $\mathbf{M}$ is the molar weight vector of the components present in the reactions. The dimensions of $\boldsymbol{\alpha}$ are $N_{rxn} \times (N_{sub} + N_{part})$, where N_{rxn} is the number of reactions present in the system, and $\mathbf{M}$ is a column vector of $(N_{sub} + N_{part})$ entries.

Reaction Kinetics

The net rate of production of all components can be expressed in terms of the stoichiometry matrix and the reaction rate vector:

$$\mathbf{W} = \boldsymbol{\alpha}^T \mathbf{r}, \tag{12}$$

where

$$\mathbf{r} = [r_1, r_2, ..., r_{N_{rxn}}]^T, \tag{13}$$

and r_i is the reaction rate of reaction i.

The rate of a given reaction depends on the participating components:

$$r_i = \prod_{j=1}^{N_{part}+N_{sub}} R_{i,j}(C_j) \tag{14}$$

where $R_{i,j}$ is the reaction kinetic expression of component j in reaction i, and C_j is the concentration of component j (soluble or particulate). The model utilizes four

types of reaction kinetics, each having a single numerical parameter ($K_{i,j}$), as follows.

- Zero order

$$R_{i,j} = K_{i,j} \tag{15}$$

- First order

$$R_{i,j} = K_{i,j} C_j \tag{16}$$

- Monod

$$R_{i,j} = \frac{C_j}{K_{i,j} + C_j} \tag{17}$$

- Inhibition

$$R_{i,j} = \frac{1}{K_{i,j} + C_j} \tag{18}$$

If component k does not participate in reaction i, then its reaction kinetic expression is zero order with $K_{i,k} = 1$. A typical reaction rate equation for a single particulate, single substrate reaction is

$$r = \mu_{max} C_{part} \frac{C_{sub}}{K_{sub} + C_{sub}}, \tag{19}$$

where μ_{max} is the maximum growth rate of the cell, and K_{sub} is the so called half saturation coefficient of the substrate in that reaction.

Detachment and Attachment

Biofilm accumulation on solid surfaces is the net result of many physical and chemical processes, including

- Adsorption. Cells attach to the substratum surface. This can be reversible or irreversible.
- Desorption. Absorbed cells can leave the substratum, and enter the bulk compartment.
- Attachment. Cells in the bulk compartment attach to an already existent biofilm.
- Detachment. A single cell or a group of cells leave the biofilm.

In our model we assume the existence of an initial layer of biofilm, thus adsorption and desorption are not included in the model.

Attachment and adsorption are very similar processes, with the exception that in attachment cells are captured by the film, while in adsorption the capturing medium is the substratum.

Detachment can be either erosion or sloughing. Erosion refers to a continuous loss of a small amount of biofilm, while sloughing means rapid, massive loss of biomass.

The model utilizes a net detachment expression,

$$net\ detachment = detachment - attachment.$$

This expression describes the net flux of particulate mass leaving the biofilm surface. It is also important to note that this process is assumed to be present at the interface only, which might not be a correct assumption. In biofilm research the important parameters that determine the magnitude of detachment/attachment is an open research topic. The model assumes the interfacial flux of particulate mass is a quadratic function of the biofilm thickness,

$$R_{det} = a_2 L_f^2 + a_1 L_f + a_0. \tag{20}$$

Positive flux means detachment, while negative flux means attachment.

Advection and Diffusion

In a pipeline system advection moves components in the flow direction, and the growth of the biofilm imposes an advective motion on the particles in the film.

The streamwise flow can be turbulent or laminar, which determines the velocity profiles in the pipe, as well as the diffusion coefficients.

Diffusion occurs both in the radial and axial direction. The axial diffusion is typically orders of magnitude smaller than the advection in the same direction, thus

it can be omitted. Diffusion in the radial direction is a very important phenomenon. It transfers soluble and particulate components to and from the center of the pipe and into the film. The rate of diffusion is determined by the flow regime. In laminar flow the diffusion coefficient of a given component in the pipe is equal to the molecular diffusion of the component, while in turbulent flow conditions the diffusion coefficient varies from the eddy diffusion to the molecular one as particles move from the center of the pipe towards the wall of the pipe. An empirical formula for determining the eddy diffusivity is given in [1].

CHAPTER 3

GOVERNING EQUATIONS

The governing equations for both the bulk liquid and biofilm compartments are based on the conservation of mass principle,

$$accumulation\,rate + transport = production.$$

Using the notation introduced in the previous sections,

$$\frac{\partial}{\partial t}\int\int\int_V \mathbf{Q}\,dV + \oint_S (\mathbf{S} - \mathbf{S}_v)\,\mathbf{n}\,dS = \int\int\int_V \mathbf{W}\,dV, \tag{21}$$

where $\mathbf{S}$ represents the inviscid (convective) and $\mathbf{S}_v$ represents the viscous fluxes, $\mathbf{W}$ is the vector of source terms (reactions), V is any arbitrary volume in the system, S is the surrounding surface of volume element V, and $\mathbf{n}$ is the normal of the infinitesimal surface dS. In the bulk compartment $\mathbf{Q}$ is the vector of concentrations of all components (N_{sub} substrates and N_{part} particulates). In the film compartment,

$$\mathbf{Q} = \begin{pmatrix} \varepsilon_l C_1 \\ \vdots \\ \varepsilon_l C_{N_{sub}} \\ \varepsilon_1 \varrho_{1+N_{sub}} \\ \vdots \\ \varepsilon_{N_{part}} \varrho_{N_{part}-1+N_{sub}} \end{pmatrix}. \tag{22}$$

The reason for including only $N_{part} - 1$ particulate components in $\mathbf{Q}$ is due to the constraint

$$\sum_{i=1}^{N_{part}} \varepsilon_i + \varepsilon_l = 1. \tag{23}$$

The size of all vectors in the biofilm compartment is $N_{sub} + N_{part} - 1$. Now the form of $\mathbf{S}$ and $\mathbf{S}_v$ has to be determined. The vector of inviscid fluxes in the bulk compartment is the following:

$$\mathbf{S} = \begin{pmatrix} \varepsilon_l C_i (\mathbf{u} - \mathbf{u_v}) \\ \vdots \\ \varepsilon_l C_{N_{sub}} (\mathbf{u} - \mathbf{u_v}) \\ \varepsilon_l C_{N_{sub}+1} (\mathbf{u} - \mathbf{u_v}) \\ \vdots \\ \varepsilon_l C_{N_{sub}+N_{part}} (\mathbf{u} - \mathbf{u_v}) \end{pmatrix} \tag{24}$$

where C_i is the concentration of substrates and particulates, $\mathbf{u}$ is the imposed velocity profile, and $\mathbf{u_v}$ is the velocity with which the control surface S is moving. Thus $\mathbf{u} - \mathbf{u_v}$ is the velocity of the liquid relative to the coordinate system. The direction of the flow is in the axial (x) direction. The shape of the imposed velocity profile depends on the flow regime. In laminar flow a parabolic profile is assumed:

$$u(y) = u_{max} \frac{y - y_B}{R - y_B} (2 - \frac{y - y_B}{R - y_B}), \tag{25}$$

where R is the radius of the pipe, y_B is the thickness of the biofilm, y is the coordinate in the radial direction, $u(y)$ is the magnitude of the velocity, and u_{max} is calculated from the flowrate using

$$u_{max} = 2\frac{q}{A}, \tag{26}$$

where q is the flowrate and A is the area of the cross-section. In the case of turbulent flow, the velocity profile is given by

$$u(y) = u_{max}(\frac{y - y_B}{R - y_B})^{\frac{1}{n}}, \tag{27}$$

where

$$u_{max} = \frac{q}{A}\frac{(n+1)(n+2)}{2n^2} \text{ and}$$
$$n = n(Re) \approx 7. \tag{28}$$

The vector of viscous fluxes in the bulk compartment, in accordance with Fick's law is

$$\mathbf{S}_v = \begin{pmatrix} D_1 \nabla C_1 \\ \vdots \\ D_{N_{sub}} \nabla C_{N_{sub}} \\ D_{N_{sub}+1} \nabla C_{N_{sub}+1} \\ \vdots \\ D_{N_{sub}+N_{part}} \nabla C_{N_{sub}+N_{part}} \end{pmatrix}, \tag{29}$$

where D_i is the diffusion coefficient of component i. The coefficient D_i is the function of the flow regime (laminar or turbulent) and the spatial coordinates; i.e.

$$D_i = D_i(Re, x, y, z), \tag{30}$$

where Re is the Reynolds number. For laminar flow conditions D_i is equal to the molecular diffusion of component i, while under turbulent conditions D_i varies from a large turbulent diffusion coefficient in the bulk to molecular diffusion in the boundary

layer. The inviscid and viscous fluxes in the film compartment are different from those in the bulk,

$$\mathbf{S} = \begin{pmatrix} -\varepsilon_l C_1 \mathbf{u_v} \\ \vdots \\ -\varepsilon_l C_{N_{sub}} \mathbf{u_v} \\ \varepsilon_1 \varrho_1 (\mathbf{u_s} - \mathbf{u_v}) \\ \vdots \\ \varepsilon_{N_{part}-1} \varrho_{N_{part}-1} (\mathbf{u_s} - \mathbf{u_v}) \end{pmatrix} \text{ and}$$

$$\mathbf{S}_v = \begin{pmatrix} D_{F1} \nabla C_1 \\ \vdots \\ D_{FN_{sub}} \nabla C_{N_{sub}} \\ 0 \\ 0 \\ \vdots \\ 0 \end{pmatrix}, \tag{31}$$

where $\mathbf{u}_s$ is the solid velocity of the particulates. The vectors $\mathbf{S}$ and $\mathbf{S}_v$ reflect the assumptions that (a) soluble components do not get displaced as the solid phases move and (b) particulate components do not diffuse inside the film compartment. Since the diffusional resistance inside the film is typically greater than that in the bulk, different diffusion coefficients are used (D_{Fi}). These coefficients are calculated from the molecular ones using an appropriate constant D_{bb} and the formula

$$D_{Fi} = D_{bb} D_i. \tag{32}$$

In the above vectors the value of $\mathbf{u_s}$ is unknown. This can be determined if we write the governing equations for the N_{part} particulates, divide them by ϱ_i and sum them

using a *fixed volume* ($u_v = 0$)

$$\oint_S \mathbf{u}_s \mathbf{n}\, dS = \frac{1}{1-\varepsilon_l} \int\int\int_V \left(\sum_{i=1}^{N_{part}} \frac{W_{N_{sub}+i}}{\varrho_i}\, dV \right), \tag{33}$$

or in differential form (using Gauss' theorem)

$$\nabla \mathbf{u_s} = \frac{1}{1-\varepsilon_l} \sum_{i=1}^{N_{part}} \frac{W_{N_{sub}+i}}{\varrho_i}. \tag{34}$$

To determine the magnitude and direction of $\mathbf{u_s}$ these equations are not sufficient. However, the biofilm growth is assumed to be one dimensional, perpendicular to the pipe wall. Thus, the previous equation can be simplified as

$$\frac{du_s}{dy} = \frac{1}{1-\varepsilon_l} \sum_{i=1}^{N_{part}} \frac{W_{N_{sub}+i}}{\varrho_i}. \tag{35}$$

This equation can be solved with the initial condition $u_s = 0$ at the solid wall.

To solve the governing equations described above, appropriate boundary conditions are needed. At the solid wall the fluxes are zero, since we assume that no corrosion exists. Due to the axisymmetry of the problem, at the centerline the boundary condition is

$$\left. \frac{\partial \mathbf{Q}}{\partial n} \right|_{axis} = 0. \tag{36}$$

The inlet conditions are specified, while the outlet conditions are extrapolated from the interior solutions.

The last problem to consider is the treatment of the bulk liquid-biofilm interface. This interface moves in time as the film grows/shrinks. Using the control surface

ideas mentioned earlier, describing the interface behavior is fairly straightforward. Two coinciding volume elements, one in the bulk and one in the film compartment, can be separated by the interface at all times. This means that the volumes will move and deform in time to follow the interface movement. Characklis et al. [4] derives the interface boundary condition,

$$[(\mathbf{S} - \mathbf{S}_v) \cdot \mathbf{n_I}]_B - [(\mathbf{S} - \mathbf{S}_v) \cdot \mathbf{n_I}]_F = (\mathbf{R}_F \cdot \mathbf{n_I}), \tag{37}$$

where R_F denotes the surface production of components, n_I is the normal to the interface, and indices B and F mean bulk and film, respectively. There are three special cases: (a) soluble components, (b) particulates in the bulk at the interface, and (c) particulates in the film. Since there is no surface production of substrates at the interface, and the advective velocity is also 0, the following boundary condition holds for substrates,

$$-\mathbf{u_v} \cdot \mathbf{n_I}(\varepsilon_l C_i)_B - [D_i \nabla C_i \cdot \mathbf{n_I}]_B = -\mathbf{u_v} \cdot \mathbf{n_I}(\varepsilon_l C_i)_F - [D_i \nabla C_i \cdot \mathbf{n_I}]_F. \tag{38}$$

The expression for the particulate components in the bulk compartment (no film contributions) is

$$(\mathbf{u} - \mathbf{u_v}) \cdot \mathbf{n_I}(\varepsilon_l C_i)_B - [D_i \nabla C_i \cdot \mathbf{n_I}]_B = [(\mathbf{R}_i)_F \cdot \mathbf{n_I}]. \tag{39}$$

The boundary condition for the particulates in the film has a similar form (no bulk contributions and no diffusion in the film),

$$-(\mathbf{u}_s - \mathbf{u_v}) \cdot \mathbf{n_I}(\varepsilon_i \varrho_i)_F = [(\mathbf{R}_i)_F \cdot \mathbf{n_I}]. \tag{40}$$

This boundary condition applies to all but one particulate component. The last equation can be used to determine $\mathbf{u_v}$ at the interface $(\mathbf{u_v})_I$. After some algebra,

$$(\mathbf{u_v})_I = \mathbf{u}_s + \frac{1}{1-\varepsilon_l} \sum_{i=1}^{N_{part}} \frac{(\mathbf{R}_i)_F}{\varrho_i}. \tag{41}$$

This final result gives us an expression for the change in biofilm thickness L_F, since

$$\frac{dL_F}{dt} = (u_v)_I, \tag{42}$$

where $(u_v)_I$ is the magnitude of the interface velocity.

This system of equations is well-posed, and using a numerical technique to be described in the following section, allows the investigation of important biofilm processes.

CHAPTER 4

NUMERICAL TECHNIQUE

The general form of the governing equations and the boundary conditions are discretized and advanced in time using the finite volume approach. The physical space is divided into a (large) number of control volumes (see Fig. 2, and the volume averaged values of $\mathbf{Q}$ are determined in each control volume. Since the problem at hand is axisymmetric, and a structured grid is used, a general indexing scheme can be utilized. Two indices will suffice to describe axisymmetric domains, where the first index (i) spans the "columns" of the domain, and the second index (j) spans the "rows". "Rows" are approximately aligned with the direction of the flow (axial direction), and "columns" go from the centerline to the pipe wall (radial direction). The discretized version of the governing equation for volume (i, j) is

$$\begin{aligned}\frac{\partial(\mathbf{Q}_{ij}V_{ij})}{\partial t} + \Big[&(\mathbf{S}-\mathbf{S}_v)_{i+1/2,j}\cdot\mathbf{n}_{i+1/2,j}S_{i+1/2,j} - \\ &(\mathbf{S}-\mathbf{S}_v)_{i-1/2,j}\cdot\mathbf{n}_{i-1/2,j}S_{i-1/2,j} + \\ &(\mathbf{S}-\mathbf{S}_v)_{i,j+1/2}\cdot\mathbf{n}_{i,j+1/2}S_{i,j+1/2} - \\ &(\mathbf{S}-\mathbf{S}_v)_{i,j-1/2}\cdot\mathbf{n}_{i,j-1/2}S_{i,j-1/2}\Big] = \mathbf{W}_{ij}V_{ij},\end{aligned} \tag{43}$$

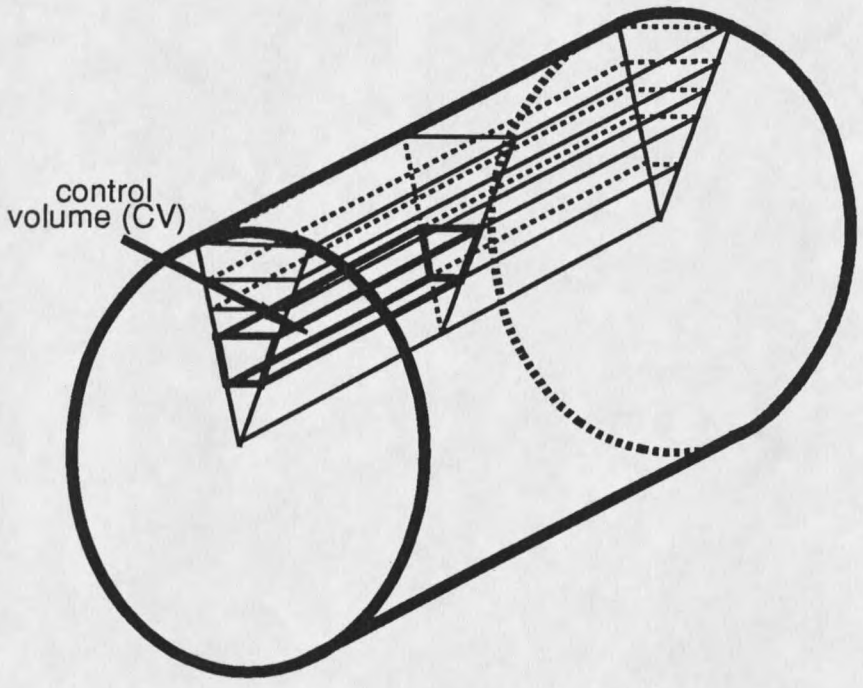

Figure 2: The discretized spatial domain.

where $\mathbf{Q}_{ij}$ and $\mathbf{W}_{ij}$ are the volume averaged values of $\mathbf{Q}$ and $\mathbf{W}$,

$$\mathbf{Q_{ij}} = \frac{1}{V_{ij}} \int\int\int_{V_{ij}} \mathbf{Q} dV, \tag{44}$$

$$\mathbf{W_{ij}} = \frac{1}{V_{ij}} \int\int\int_{V_{ij}} \mathbf{W} dV. \tag{45}$$

Similarly, $\mathbf{n}_{i\pm1/2,j}$ and $\mathbf{n}_{i,j\pm1/2}$ are the surface normals of the four surfaces enclosing volume element V_{ij}, and the surface averaged fluxes for the four surfaces are

$$(\mathbf{S} - \mathbf{S}_v)_{i\pm1/2,j} = \frac{1}{S_{i\pm1/2,j}} \oint_{S_{i\pm1/2,j}} (\mathbf{S} - \mathbf{S}_v) dS, \tag{46}$$

$$(\mathbf{S} - \mathbf{S}_v)_{i,j\pm1/2} = \frac{1}{S_{i,j\pm1/2}} \oint_{S_{i,j\pm1/2}} (\mathbf{S} - \mathbf{S}_v) dS. \tag{47}$$

To simplify the notation, the flux and source terms are grouped into a residual, and

thus (43) has the form:

$$\frac{\partial(\mathbf{Q}_{ij}V_{ij})}{\partial t} + \mathbf{R}_{ij} = 0, \tag{48}$$

where

$$\begin{aligned}\mathbf{R}_{ij} = \Big[&(\mathbf{S}-\mathbf{S}_v)_{i+1/2,j}\cdot\mathbf{n}_{i+1/2,j}S_{i+1/2,j} - \\ &(\mathbf{S}-\mathbf{S}_v)_{i-1/2,j}\cdot\mathbf{n}_{i-1/2,j}S_{i-1/2,j} + \\ &(\mathbf{S}-\mathbf{S}_v)_{i,j+1/2}\cdot\mathbf{n}_{i,j+1/2}S_{i,j+1/2} - \\ &(\mathbf{S}-\mathbf{S}_v)_{i,j-1/2}\cdot\mathbf{n}_{i,j-1/2}S_{i,j-1/2}\Big] - \mathbf{W}_{ij}V_{ij}.\end{aligned} \tag{49}$$

Equation (48) is advanced in time using a general three point integration formula [8]:

$$\frac{(1+\psi)\Delta(\mathbf{Q}V)^n_{ij} - \psi\Delta(\mathbf{Q}V)^{n-1}_{ij}}{\Delta t^n} = (\theta-1)\mathbf{R}^n_{ij} - \theta\mathbf{R}^{n+1}_{ij}, \tag{50}$$

where $\Delta(\cdot)$ is the forward difference operator, defined as

$$\Delta(\cdot) = (\cdot)^{n+1} - (\cdot)^n \tag{51}$$

and ψ, θ are parameters that determine the integration scheme to be used. For example, $\psi = \theta = 0$ corresponds to the classical forward Euler integration formula, $\psi = 0$ and $\theta = 1$ results in the backward Euler scheme. For $\theta = 0$ the integration can be performed without any difficulty, since the unknowns $\mathbf{Q}^{n+1}$ are present on the left hand side only. For $\theta \neq 0$ both the left and the right hand side contain the unknowns $\mathbf{Q}^{n+1}$, and thus the equation becomes nonlinear. In this paper we choose Newton's

Method to linearize the equations and find the solution using a number of iterative steps. In order to apply Newton's Method, the equation has to have the form of $f(x) = 0$. This form for (50) is

$$L(\mathbf{Q}^{n+1}) = \frac{(1+\psi)\Delta(\mathbf{Q}V)_{ij}^{n} - \psi\Delta(\mathbf{Q}V)_{ij}^{n-1}}{\Delta t^n} - \left[(\theta-1)\mathbf{R}_{ij}^{n} - \theta\mathbf{R}_{ij}^{n+1}\right] = 0. \qquad (52)$$

The linear scheme is then

$$L'(\mathbf{Q}^P)\Delta\mathbf{Q}^P = -L(\mathbf{Q}^P), \qquad (53)$$

where P is the iteration index. Thus $\mathbf{Q}^{P=0} = \mathbf{Q}^n$, and $\mathbf{Q}^{P\to\infty} = \mathbf{Q}^{n+1}$. The expression of L is complicated by the fact that the volume elements change in time. The model utilizes the *Geometric Conservation Law* [6],[11]:

$$L(\mathbf{Q}^P) = \frac{V_{ij}^{P+1}(\mathbf{Q}_{ij}^{P} - \mathbf{Q}_{ij}^{n})}{\Delta t^n} - \frac{\psi}{1+\psi}\frac{V_{ij}^{n-1}\Delta(\mathbf{Q}_{ij}^{n-1})}{\Delta t^n} + \frac{\mathbf{Q}_{ij}^{n}}{1+\psi}\left[(\theta-1)\hat{\mathbf{R}}_{ij}^{n} - \theta\hat{\mathbf{R}}_{ij}^{P}\right] - \frac{1}{1+\psi}\left[(\theta-1)\mathbf{R}_{ij}^{n} - \theta\mathbf{R}_{ij}^{P}\right], \qquad (54)$$

where $\hat{\mathbf{R}}_{ij}$ is the "geometric residual"

$$\hat{\mathbf{R}}_{ij} = -\Big[\mathbf{u}_v \cdot \mathbf{n}_{i+1/2,j}S_{i+1/2,j} - \mathbf{u}_v \cdot \mathbf{n}_{i-1/2,j}S_{i-1/2,j} + \mathbf{u}_v \cdot \mathbf{n}_{i,j+1/2}S_{i,j+1/2} - \mathbf{u}_v \cdot \mathbf{n}_{i,j-1/2}S_{i,j-1/2}\Big]. \qquad (55)$$

To determine the first derivative of $L(\mathbf{Q})$ we make the simplifying assumption that the geometric residual does not depend on the vector of unknowns $\mathbf{Q}^P$. This significantly reduces the complexity. Although the assumption is not true, the dependence is very

slight. Using this assumption,

$$L'(\mathbf{Q}^P) = \frac{V_{ij}^{P+1}}{\Delta t^n}\mathbf{I}_{ij} + \frac{\theta}{1+\psi}\frac{\partial \mathbf{R}_{ij}^P}{\partial \mathbf{Q}}, \tag{56}$$

where

$$\begin{aligned}\frac{\partial \mathbf{R}_{ij}}{\partial \mathbf{Q}} = \big[&(\mathbf{D}-\mathbf{D}_v)_{i+1/2,j}\cdot \mathbf{n}_{i+1/2,j}S_{i+1/2,j} - \\ &(\mathbf{D}-\mathbf{D}_v)_{i-1/2,j}\cdot \mathbf{n}_{i-1/2,j}S_{i-1/2,j} + \\ &(\mathbf{D}-\mathbf{D}_v)_{i,j+1/2}\cdot \mathbf{n}_{i,j+1/2}S_{i,j+1/2} - \\ &(\mathbf{D}-\mathbf{D}_v)_{i,j-1/2}\cdot \mathbf{n}_{i,j-1/2}S_{i,j-1/2}\big] - \frac{\partial \mathbf{W}_{ij}}{\partial \mathbf{Q}}V_{ij}.\end{aligned} \tag{57}$$

In the above equations $\mathbf{I}$ is the identity matrix, and $\mathbf{D}$ and $\mathbf{D}_v$ are the inviscid and viscous Jacobians, respectively. The indices of the Jacobians denote that the matrices multiply vectors $\Delta\mathbf{Q}$ at the same locations, e.g. $\mathbf{D}_{i+1/2,j}$ multiplies $\Delta\mathbf{Q}_{i+1/2,j}$.

Our next task is to determine the surface averaged values of $\Delta\mathbf{Q}$. This can be done by extrapolating the volume averaged values to the surfaces. Two extrapolations exist, one from the "right" (positive) and one from the "left" (negative) [12]; that is,

$$\mathbf{Q}_{l\mp 1/2}^{\pm} = \mathbf{Q}_l \mp \frac{\phi}{4}[(1\pm\kappa)(\mathbf{Q}_l - \mathbf{Q}_{l-1}) + (1\mp\kappa)(\mathbf{Q}_{l+1}-\mathbf{Q}_l)], \tag{58}$$

where l is a generic index for i or j, depending on the direction of the interpolation. Values of ϕ and κ determine the order and type of the interpolation formula. If $\phi = 0$ is selected, then the resulting extrapolation formula is first-order upwind,

$$\mathbf{Q}_{l\mp 1/2}^{\pm} = \mathbf{Q}_l. \tag{59}$$

Other parameter choices result in second-order upwind, second order central differences and third-order upwind-biased extrapolation [7]. For simplicity first-order upwind extrapolations are used in this paper.

Using the left and right extrapolation values, the inviscid fluxes (using general index l) are given by

$$\mathbf{S}^{\pm}_{l+1/2} \cdot \mathbf{n}_{l+1/2} = \frac{\tilde{\mathbf{u}}^{\mp}_{l+1/2} \pm |\tilde{\mathbf{u}}^{\mp}_{l+1/2}|}{2} \mathbf{Q}^{\mp}_{l+1/2}, \tag{60}$$

where $\tilde{\mathbf{u}}$ is component of the relative velocity normal to the surface $l + 1/2$

$$\tilde{\mathbf{u}}_{l+1/2} = (\mathbf{u} - \mathbf{u}_v)_{l+1/2} \cdot \mathbf{n}_{l+1/2}. \tag{61}$$

To determine $\mathbf{u}$ at the surfaces, the same extrapolation formulas can be used as described in eq. 58. Note that in the biofilm, $\mathbf{u}_s$ and $\mathbf{u}_v$ are known at the surfaces, so the trivial extrapolation $(\cdot)^{+}_{l+1/2} = (\cdot)^{-}_{l+1/2} = (\cdot)_{l+1/2}$ can be used. A similar expression can be derived for the inviscid Jacobians, yielding

$$\tilde{\mathbf{D}}_{l+1/2} \Delta \mathbf{Q}_{l+1/2} = \tilde{\mathbf{D}}^{+}_{l+1/2} \Delta \mathbf{Q}_{l} + \tilde{\mathbf{D}}^{-}_{l+1/2} \Delta \mathbf{Q}_{l+1}, \tag{62}$$

where the first-order extrapolation formula for $\Delta \mathbf{Q}_{l+1/2}$ has been utilized, and the generalized Jacobian matrix $\tilde{\mathbf{D}} = \mathbf{D} \cdot \mathbf{n}$ has been introduced.

The viscous fluxes can be determined from the directional derivative of the concentration, thus for component k it has the form

$$(\tilde{\mathbf{S}}_v)_k = (D_k)_{l+1/2} \mathbf{n}_{l+1/2} \cdot \nabla C_k = (D_k)_{l+1/2} \frac{dC_k}{dn_{l+1/2}}. \tag{63}$$

Diffusion coefficient $(D_k)_{l+1/2}$ is determined as the average of the diffusion coefficients of the volumes that share the surface under consideration. The above equation can be simplified, if we assume that the axial diffusion is insignificant,

$$(D_k)_{l+1/2}\frac{dC_k}{dn_{j+1/2}} = (D_k)_{j+1/2}|\nabla\eta|_{j+1/2}\frac{\partial C_k}{\partial\eta}_{j+1/2}, \tag{64}$$

where η represents the generalized curvilinear coordinate in the j direction. The components of the above equation can easily be determined from known concentrations and volume elements from the relationships

$$\left(\frac{\partial C_k}{\partial\eta}\right)_{j+1/2} = (C_k)_{j+1} - (C_k)_j \text{and}$$
$$|\nabla\eta|_{j+1/2} = \frac{S_{j+1/2}}{0.5(V_j + V_{j+1})}. \tag{65}$$

In words, $|\nabla\eta|$ is determined as the ratio of the surface of interest and the volumes sharing that surface. Similarly to the inviscid Jacobians, the viscous Jacobians can be written as the sum of "positive" and "negative" contributions,

$$(\tilde{\mathbf{D}}_v)_{j+1/2}\Delta\mathbf{Q}_{j+1/2} = (\tilde{\mathbf{D}}_v)^+_{j+1/2}\Delta\mathbf{Q}_j + (\tilde{\mathbf{D}}_v)^-_{j+1/2}\Delta\mathbf{Q}_{j+1}, \tag{66}$$

where

$$(\tilde{\mathbf{D}}_v)^\pm_{j\pm1/2} = \mp D_{j\pm1/2}|\nabla\eta|_{j\pm1/2}\left(\frac{1}{\varepsilon_l}\right)_j \mathbf{I}. \tag{67}$$

The source term and its Jacobian remain to be specified. The form of the source term is given in equation (12). The Jacobian can be calculated in a straightforward manner using (12) and (14) - (18).

Substituting the expressions for fluxes, source terms and their Jacobians into (53) results in a set of coupled linear equations for $\Delta\mathbf{Q}^P$. These equations written for $\Delta\mathbf{Q}^P$ in volume (i,j) will have contributions from itself, and also from volumes $(i+1,j)$, $(i-1,j)$, $(i,j-1)$, $(i,j+1)$. However, after a closer inspection of the contribution of $(i+1,j)$ we can conclude that it is zero for positive flow velocities. Thus we can perform a marching algorithm, meaning that we solve the equations for volumes in the ith column, and then repeat the procedure for the next column. The next column is $i+1$ for positive flow fields (which is typically the case), and $i-1$ for negative flows. Further simplification of the equations results from the marching algorithm. The contribution of $(i-1,j)$ is zero, since the previous column already converged, thus $\Delta\mathbf{Q}_{i-1,j} = 0$. As a result, at every column a block-tridiagonal system of equations has to be solved. The block-size is $N_{sub} + N_{part}$ in the bulk, and $N_{sub} + N_{part} - 1$ in the film. Recursive techniques, such as the block Thomas algorithm ([8]) can be used effectively to solve this system of equations.

The two remaining quantities that have to be determined are $\mathbf{u}_s$ and $\mathbf{u}_v$. If we assume that the streamwise direction is perpendicular to the normal of the solid wall, a discretized version of (33) is

$$[u_s(\mathbf{e}_{u_s}\cdot\mathbf{n})S]_{i,j+1/2} - [u_s(\mathbf{e}_{u_s}\cdot\mathbf{n})S]_{i,j-1/2} = \frac{1}{1-\varepsilon_l}\left(\sum_{k=1}^{N_{part}}\frac{W_{Nsub+k}}{\varrho_k}\right), \qquad (68)$$

where $\mathbf{e}_{u_s}$ is the unit vector of $\mathbf{u}_s$. This equation can be solved for u_s starting from the wall, where it is 0, and incrementally determine its value for each surface $S_{i,j+1/2}$

to the interface. After determining the value of u_s at the interface, $(\mathbf{u}_v)_I$ can be determined using the value of $\mathbf{R}_F$.

At this point all values are known at time n, so the next step is to determine the movement of the grid. The grid is allowed to move in the j direction (normal to the wall) only. Knowing the interface velocity $(\mathbf{u}_v)_I$, the velocities of the surfaces $S_{i,j+1/2}$ in the full domain can be determined. The velocity $\mathbf{u}_v$ linearly varies from the full value at the interface to zero at the wall and at the centerline. The velocity determined this way gives the velocity of the centroids of the surfaces, thus a further computational step is needed to determine the vertex velocities. The actual displacement of the vertices is determined by multiplying the vertex velocity with the time step. A very simple way of calculating the vertex velocities is

$$\mathbf{u}_{i+1,j+1/2} = \mathbf{u}_{i,j+1/2} + 2(\mathbf{u}_{i,j+1/2} - (\mathbf{u}_v)_{i+1/2,j+1/2}), \text{ and}$$

$$\mathbf{u}_{0,j+1/2} = (\mathbf{u}_v)_{1/2,j+1/2}, \tag{69}$$

where $\mathbf{u}_{i,j+1/2}$ is the vertex velocity of the "left" end of surface $S_{i+1/2,j+1/2}$, $\mathbf{u}_{i+1,j+1/2}$ is the vertex velocity of the "right" end of the same surface, and $(\mathbf{u}_v)_{i+1/2,j+1/2}$ is the known centroid velocity of the same surface. The velocity of the very first vertex has to be determined using the second part of the equation, or some other additional information. The disadvantage of the above method of determining the velocity of the first vertex is that this way a "jagged" grid can be produced, if the growth of the film is uneven (Figure 3).

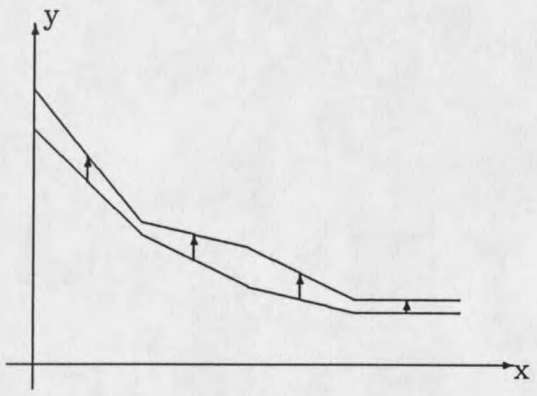

Figure 3: Grid resulting from uneven growth

Grid Generation

There are a few general heuristics that can be employed in generating an appropriate grid. First of all, we would like to resolve soluble profiles in the biofilm, and since its thickness is in the 10-100 micron range, a fine grid (few micron spacing) is necessary. On the other hand, the profiles of soluble and particulate components in the bulk are not expected to change significantly far from the film. Near the film we would like to have similar resolution to that in the film, and these two requirements call for a variable sized grid in the bulk. In this model the initial grid in the bulk is given by

$$r_n = \Delta r_0 q^{n-1}, \tag{70}$$

where r_n is the spacing between the $n-1$st and nth grid in the bulk, Δr_0 is the given distance of the first grid from the bulk/film interface, and q is the quotient of the geometric series. Parameters Δr_0, q and the number of grids in the bulk (N_{rad}) have

to satisfy

$$R - L_f(0) = \sum_{n=1}^{N_{rad}} r_n, \tag{71}$$

where R is the radius of the pipe, and $L_f(0)$ is the given initial thickness of the film. Using these equations one can use one of three methods:

1. q and N_{rad} are given. In this case Δr_0 is unknown, and can be expressed as:

$$\Delta r_0 = (R - L_f(0))\frac{q-1}{q^{N_{rad}}-1} \tag{72}$$

2. q and Δr_0 are given. The unknown is N_{rad}, and can be found using a search:

$$\sum_{n=1}^{N_{rad}+1} r_n \leq R - L_f(0) \leq \sum_{n=1}^{N_{rad}} r_n \tag{73}$$

   Since N_{rad} is an integer valued number, it is not guaranteed that equality can be satisfied. Thus this method is not recommended.

3. Δr_0 and N_{rad} are given. In order to determine a suitable q a nonlinear equation has to be solved, thus Newton's Method can be used.

The advantage of option 1 is that a fairly smooth volume change can be guaranteed in the bulk ($q \approx 1$). The disadvantage is that there might be a sudden change in volumes at the film/liquid interface. On the other hand, option 3 would allow smooth change at the interface, but can result in a very coarse grid in the bulk. Unfortunately, option two would be the best, but its inaccuracy cannot be tolerated. A fourth option could use option two to determine N_{rad}, and then use option one or option three to refine

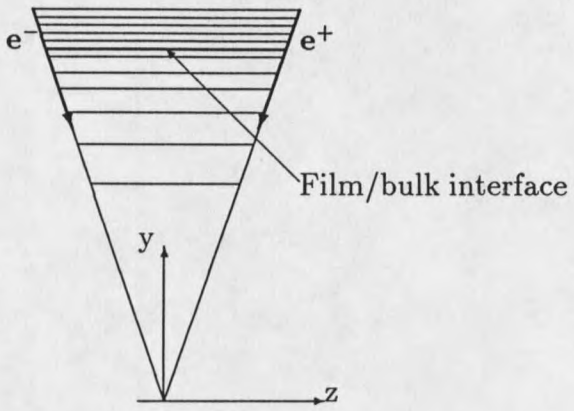

Figure 4: Section of the grid looking from the inlet

Δr_0 or q, respectively. Present implementation employs the third option. Once r_n is calculated, we can determine the vertex coordinates using

$$\mathbf{r}_n^+ = \mathbf{r}_{n-1} + r_n \mathbf{e}^+ \text{ and}$$

$$\mathbf{r}_n^- = \mathbf{r}_{n-1} + r_n \mathbf{e}^-, \tag{74}$$

where $\mathbf{e}^+$ and $\mathbf{e}^-$ are the two unit vectors of the pipe section (see Figure 4). Given the vertices of a surface, fairly simple techniques can be used to estimate the area vector. If $\mathbf{r}_{i1}$,$\mathbf{r}_{i2}$, $\mathbf{r}_{i3}$,$\mathbf{r}_{i4}$ are the vertices of surface i in clockwise order, then

$$\mathbf{S}_i \simeq [(\mathbf{r}_{i4} - \mathbf{r}_{i2}) \times (\mathbf{r}_{i3} - \mathbf{r}_{i1})]/2 \tag{75}$$

gives an estimate of the area vector. Note that in general four points do not lie on a plane, and that is the reason this equation is only an estimate for the area. However, present implementation forces the four vertices to lie on a plane, and thus the equation is precise.

Finally, a control volume is calculated as the sum of volumes of six pentahedrons

$$V_{i,j} = \frac{1}{3} \sum_{k=x,y,z} \left[(\mathbf{S}_{i,j}^{k+} \cdot (\mathbf{c}_{i,j}^{k+} - \mathbf{c}_{i,j}) + (\mathbf{S}_{i,j}^{k-} \cdot (\mathbf{c}_{i,j} - \mathbf{c}_{i,j}^{k-}) \right], \tag{76}$$

where $\mathbf{S}_{i,j}^{k\pm}$ is the surface closing the volume from the positive/negative direction of axis k, e.g $\mathbf{S}_{i,j}^{x+} = \mathbf{S}_{i+1/2,j}$ and $\mathbf{S}_{i,j}^{y-} = \mathbf{S}_{i,j-1/2}$, $\mathbf{c}_{i,j}$ is the center of volume (i,j) and is calculated as the average of the eight vertex vectors, and $\mathbf{c}_{i,j}^{k\pm}$ is the center of surface $\mathbf{S}_{i,j}^{k\pm}$.

CHAPTER 5

RESULTS

In this section a number of simulation runs are described and analyzed. The emphasis of this section is to show the behavior of the numerical technique as control parameters — such as the number of iterations at each time step, the size of the time step, etc.— are changed. Further research will determine the predictive capacity of the mathematical model (*model evaluation*).

In order to be able to perform the analysis, a "standard" experiment has to be defined, and all the other experiments are compared to this standard one. The important parameters of this standard are the following:

Length $= 2\,m$; Diameter $= 4 \cdot 10^{-3}\,m$; Flowrate $= 1.4 \cdot 10^{-6}\,\frac{m^3}{s}$;

$\varepsilon_l = 0.8$; $D_{bb} = 0.9$;

$N_{sub} = 1\ (glu)$; $N_{part} = 1\ (pse)$;

$D_{glu} = 6 \cdot 10^{-9}\,\frac{m^2}{s}$; $D_{pse} = 1.2 \cdot 10^{-9}\,\frac{m^2}{s}$; $\varrho_{pse} = 107000\,\frac{g}{m^3}$;

$L_f(0) = 10\,\mu$; $C_{glu}(0) = 20\,\frac{g}{m^3}$; $\varepsilon_{pse} = 0.2$;

$R_F = 5 \cdot 10^4 L_f^2\,\frac{kg\,m^2}{s}$;

$\alpha_{1,glu} = -1.78$; $R_{1,glu} = Q_{glu}(1.6 + Q_{glu})^{-1}$;

$\alpha_{1,pse} = 1$; $R_{1,pse} = 10^{-4} Q_{pse}\,\frac{kg}{m^3\,s}$;

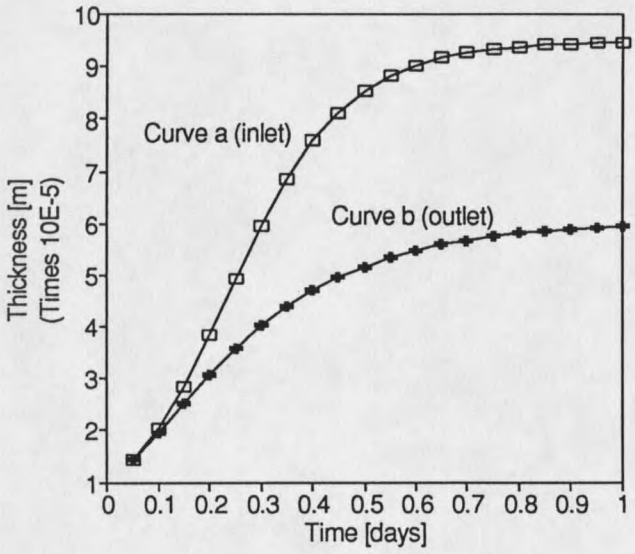

Figure 5: Standard experiment. L_f versus time

$N_{rad} = 10;\ N_{film} = 10;\ N_{axial} = 10;$

$\Delta t = 43\,s = 5 \cdot 10^{-4}\,d;$

$\kappa = 1;\ \phi = 0;\ \psi = 0;\ \theta = 1,$

where N_{film} is the number of grids in the film, N_{axial} is the number of grids in the axial direction. The geometry of the pipe and the flowrate result in a Reynolds number less than 2100; thus laminar flow regime and molecular diffusion is assumed in the pipe. The average velocity in the pipe is $v = 0.111\ m/s$. The length of an axial section is $2\,m/(N_{axial} - 1) = 0.2222\,m$. Figures 5 and 6 show the simulation results of this system. On Figure 5 the time evolution of the film thickness ($L_f(t)$)is shown. Curve a shows the thickness at the middle of the first axial section ($0.11111m$), while curve b shows that in the middle of the last axial section ($1.88889m$). It is easy to see that steady state is reached by the end of the first simulated day. In fact, another

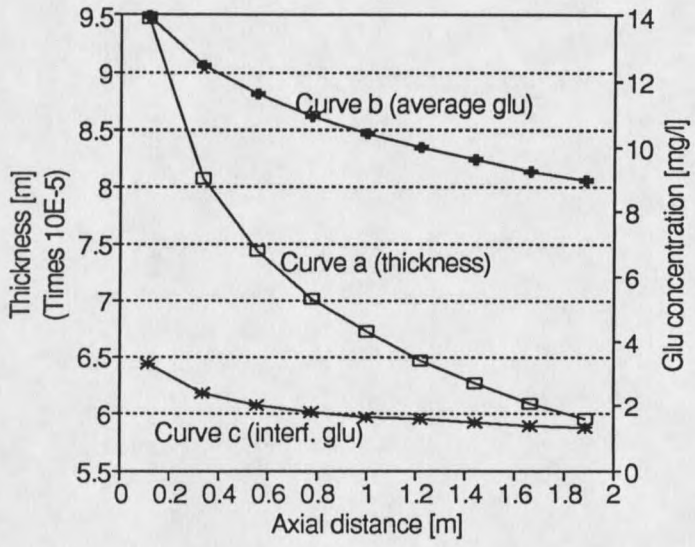

Figure 6: Standard experiment. Axial profiles

run was also performed with 6 days of simulated time, and the thickness of the film did not change more than 1%. Figure 6 shows the steady state profiles of thickness and glucose concentration as the function of axial distance from the inlet. Curve *a* shows that the thickness of the film decreases as the distance increases. The reason for this can easily be explained by looking at the other two curves. Curve *b* shows the average concentration of the only substrate, while curve *c* shows the concentration of the same component at the interface in the bulk. Since the only source of *glu* is at the inlet, it gets consumed as the liquid moves in the pipe, thus less and less "food" is available for growth down the pipe. An interesting phenomenon can also be seen on curves *b* and *c*. There is a large difference between the average and the interface concentrations, due to diffusional resistance. Since the flow regime is laminar, the diffusion coefficients are very small, and the diffusional distance is the entire radius

of the pipe. These results attest to the face validity of the model.

Size of the Time Step

The present version of the program uses fixed, user supplied time steps for integration. Thus, it is important to see how the system's accuracy changes as the time step is changed.

In this section results of two experiments are analyzed. The first experiment (run1) used a time step of $8.64s$, while the second one (run2) used $4.32s$ for time step. It is important to put these time step values into perspective. The so called CFL-numbers are widely used to determine the stability of a system of linear or nonlinear partial differential equations. Three CFL numbers can be defined in this system of equations [8]:

$$CFL_{adv} = \frac{\Delta t\, v}{\Delta x},$$

$$CFL_{diff} = \frac{\Delta t\, D}{(\Delta x)^2},$$

$$CFL_{reac} = \frac{\Delta t}{\mu_{max}},$$

where CFL_{adv} is the inviscid CFL number, CFL_{diff} is the viscous CFL number, CFL_{reac} is the reactive CFL number, Δx is the characteristic spatial resolution,

μ_{max} is the coefficient of the first order reaction rate expression. Typically, explicit integration systems are stable if CFL is less than 1. Implicit systems are usually unconditionally stable, if the partial differential equations are linear. However, if one wants to resolve a phenomenon (advection, diffusion or reaction) very accurately in time, than that CFL number has to be kept at a value less than 1. For nonlinear systems, such as this model, the CFL number can be greater than one, but in certain cases the algorithm might become unstable. In that case the time step has to be reduced. After this brief description of the CFL numbers, these numbers for the "standard" version are (at $t = 0$):

$$CFL_{adv,axial} \approx 21.7$$

$$CFL_{adv,radial} \approx 0.23$$

$$CFL_{diff} \approx 2.7 \cdot 10^5$$

$$CFL_{reac} \approx 4.6 \cdot 10^5$$

It is clear that only the radial advection (biofilm growth) is resolved in time, while the other phenomena are very sparsely sampled. Also, CFL_{diff} and CFL_{reac} are much greater than 1, thus instabilities could occur. In fact, when a time step of 86.4 s was used, the system became unstable.

Figures 7 - 9 summarize the obtained results. On Figure 7, curve a shows the time evolution of thickness at the inlet, obtained by the standard run. The curve marked $(b - a)$ shows the relative difference between the run1 and the "standard". The last curve $(c - a)$ shows the relative difference between run2 and the standard.

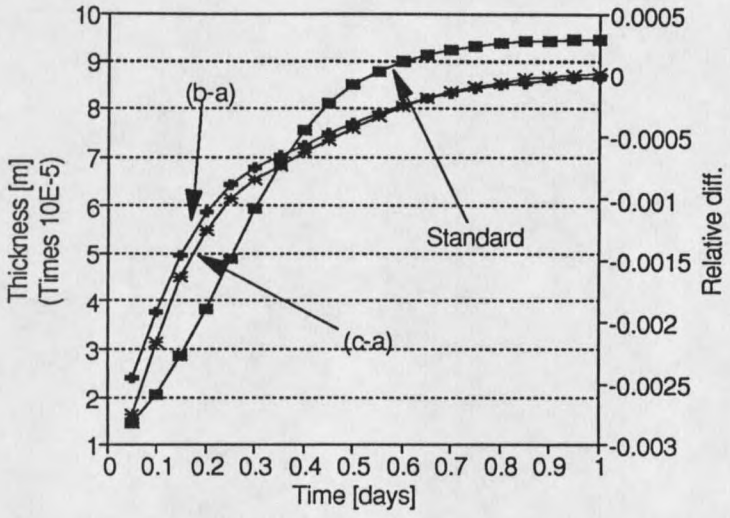

Figure 7: Difference between the standard and run1 and run2 (L_f)

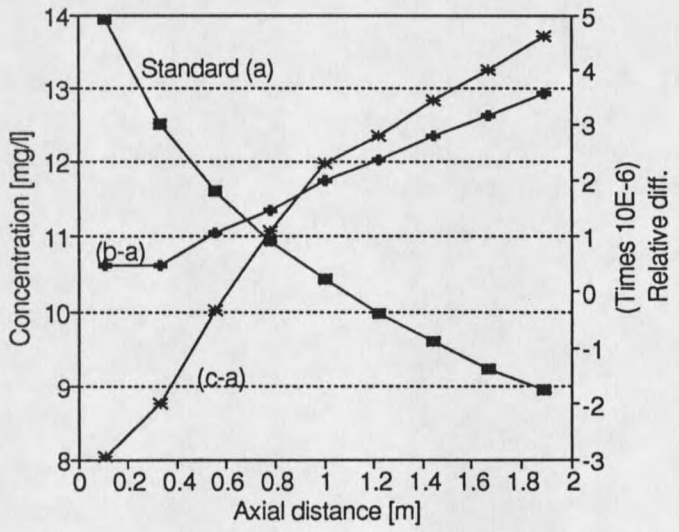

Figure 8: Difference between the standard and run1 and run2 (C_{glu}^{aver})

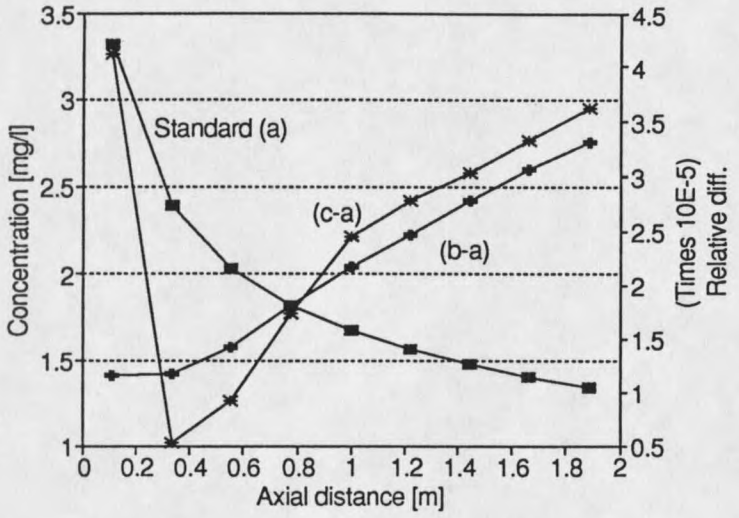

Figure 9: Difference between the standard and run1 and run2 (C_{glu}^{interf})

Some observations can be made.

- The difference approaches 0 as time progresses. The reason for this is that as the system approaches steady state, the performed Newton iterations at each time step are just refining the solution, since the time derivatives are almost 0.

- The maximum difference shown is 0.3%. However, it is not to say that this is the maximum difference between the runs. At the very first time steps one can expect even larger relative differences. (These graphs show the thickness at every 4320 seconds, thus the initial events are missing.) Since the thickness of the film is very small near the initial state, even larger *relative* differences can still mean very small *absolute* differences.

Figure 8 shows the axial profile and the relative differences of the average concen-

tration of *glu* at $t = 1day$. Curve a shows the profile obtained by the standard run. Curves $(b-a)$ and $(c-a)$ represent the relative difference between the standard and run1 and run2, respectively. Here we can see that the relative difference increases as the distance from the inlet increases. The explanation of this phenomenon is that the marching algorithm described in the previous section propagates the concentration values downstream. It is important to point out that the relative differences are very small, about 0.0005%, and their sign changes as the distance increases.

Figure 9 shows the concentration of *glu* at the interface in the bulk. Here similar observations can be made, with two exceptions: (1) The difference is constantly increasing *if* we do not consider the very first point; (2) the relative difference is an order of magnitude larger. The explanation of the latter observation is that reactions and diffusion is more rapid near the interface, thus one would expect less time accuracy as Δt increases.

Number of Iterations

Another numerical parameter in the algorithm is the number of iterations performed at each time step. One could check for convergence using some arbitrary convergence criterion, or perform a certain constant number of iterations, and then check if the result is acceptable. If not, then the time step is reduced, and the process is repeated. In the present implementation of the model the number of iterations is

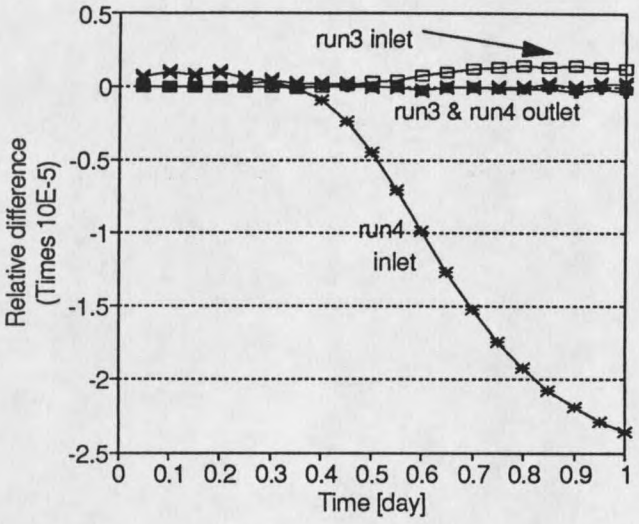

Figure 10: Difference between the standard and run3 and run4 (L_f)

fixed. The following graphs (Figure 10 and Figure 11) illustrate the obtained results (runs run3 and run4). The standard setup performs 10 iterations per time step, while run3 and run4 execute 5 and 2, respectively.

Figure 10 shows the relative difference between the thickness values at the inlet and the outlet as the function of time. The curves show the following:

- Up until 0.4 days the differences between thickness at the inlet and the outlet for both runs run3 and run4 are negligible. The explanation of this is the following. The Newton's iterations are used to determine the concentrations and volume fractions only. The grid (and thus the thickness of the film) is updated *once* per time step. This means that the difference in thickness has to come from the difference in reaction rates at a given time. The reaction rates depend on

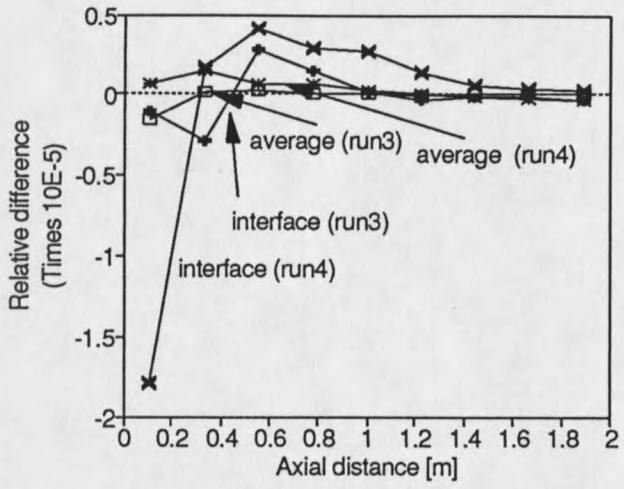

Figure 11: Difference between the standard and run3 and run4 (concentrations)

the concentration of *glu* only, since the concentration of *pse* is constant in the film. While the film is not too thick, the depletion of *glu* is not significant. Furthermore, the dependence of the reaction rate on the concentration of *glu* follows Monod kinetics, which means that for large *glu* concentrations small changes in concentration result in even smaller changes in reaction rate, because

$$\frac{dR_{1,glu}}{dQ_{glu}} = \frac{K_{1,glu}}{(K_{1,glu} + Q_{glu})^2} \text{ and}$$

$$\frac{dR_{1,glu}}{dQ_{glu}} \approx 0, \quad \text{if } Q_{glu} \gg K_{1,glu}.$$

As a result, the displacement of the grid is almost identical for the three cases.

- After 0.4 days the relative difference in inlet thickness becomes more significant. This phenomenon follows from the above explained observation. Since the film

becomes thicker as time progresses, the depletion of *glu* becomes more significant (see Figure 6), and thus the reaction rate becomes more sensitive to the concentration:

$$\frac{dR_{1,glu}}{dQ_{glu}} \approx \frac{1}{K_{1,glu}} \text{ if } Q_{glu} \leq K_{1,glu}. \tag{77}$$

Since the concentration of *glu* is greater than $K_{1,glu}$ at the inlet, the above approximation is not too accurate. Note that the relative difference at the inlet is smaller for run3 (5 iterations) than for run4 (2 iterations), which means that the iterations do reduce the error.

- The outlet thicknesses for all runs are almost identical. The explanation for this is very interesting. Due to the consumption of *glu* in the earlier sections of the pipe, the concentration of *glu* is much smaller at the outlet, even after only a few time steps. This means, however, that for practical purposes the Monod kinetic expression becomes linear, and thus only one Newton iteration would suffice to advance the integration.

Figure 11 supports the statements made above. It is obvious that the largest differences are near the inlet, which is the result of the "more" nonlinear behavior of the Monod kinetic expression. Near the outlet all concentrations are almost identical.

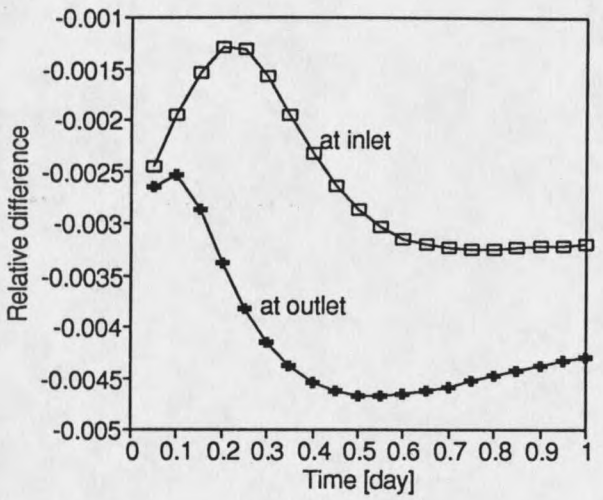

Figure 12: Difference between the standard and run5 (L_f)

Size of the Grid

Two runs were performed to test the effect of change in the size of the grid. The first run (run5) had more grid points in the bulk ($N_{rad} = 20$), while the other run (run6) had more grids in the axial direction ($N_{axial} = 19$). In order to keep the advective CFL number unchanged in the axial direction, the length of the pipe was also doubled (4m).

More Radial Grids

Figures 12 and 13 show the obtained results. Figure 12 shows a very interesting behavior. The relative difference between the thickness values as time progressed is not monotone. The difference for the inlet is about 0.2% at the beginning, then

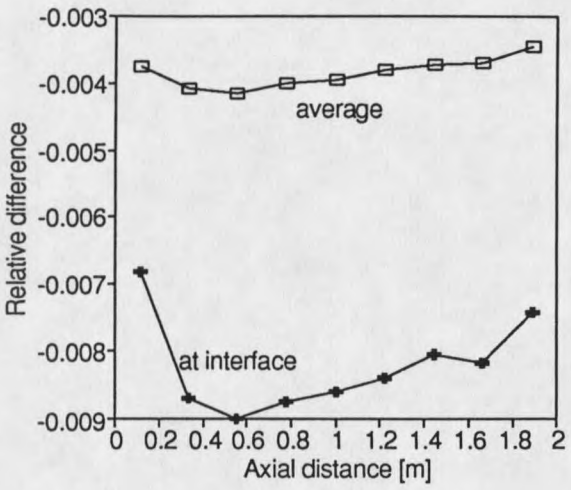

Figure 13: Difference between the standard and run5 (concentrations)

it is reduced to 0.13% at about 0.2 days, and it increases to 0.32% at 1 day. A similar, but not that emphasized, non-monotonic behavior can be observed on the outlet thickness. Here the minimum difference is reached at 0.1 days (0.25%), then the maximum difference is found at 0.5 days (0.46 %), and the final difference is 0.43% at 1 day.

Figure 13 shows the relative differences of the average concentration of *glu* and its concentration at the interface in the bulk. The average concentration of run5 differs from that of the standard by at most 0.42%, while the interface concentration differs by about 0.9%. The reason for this is the more accurate resolution of diffusion and velocity in the bulk.

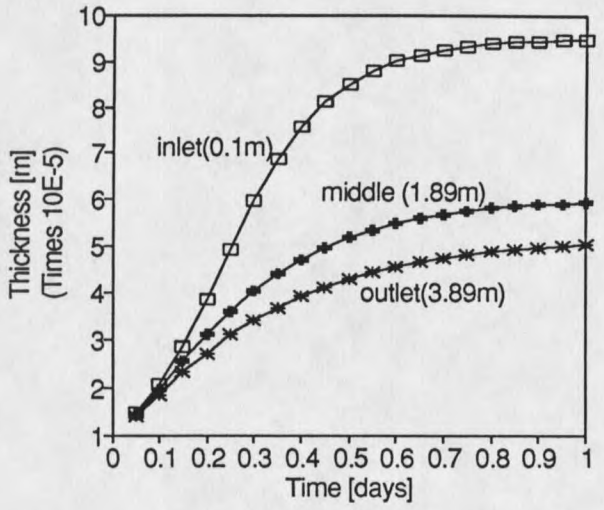

Figure 14: L_f as a function of time at the inlet, middle and outlet

More Axial Grids

Figures 14 to 17 show a few results of run6. Since the length of the pipe and the number of axial sections were doubled, the overall axial resolution did not change. This means that $CFL_{axial,adv}$ remained the same, also. It also means that the middle of the new pipe coincides with the end of the standard pipe. Figure 14 shows the time evolution of the thickness at three points in the pipe : (1) inlet, (2) middle, same as outlet of standard, and (3) outlet. Figure 15 displays the axial profile of thickness at 1 day. Both of these graphs are very similar in shape to Figure 5. More interesting observations can be made on Figures 16 and 17. Figure 16 shows the relative difference of the inlet and outlet thickness between run6 and the standard as a function of time. Note that the outlet of the standard pipe is the middle of the longer pipe. Again, a non-monotonic behavior can be seen at the inlet. However,

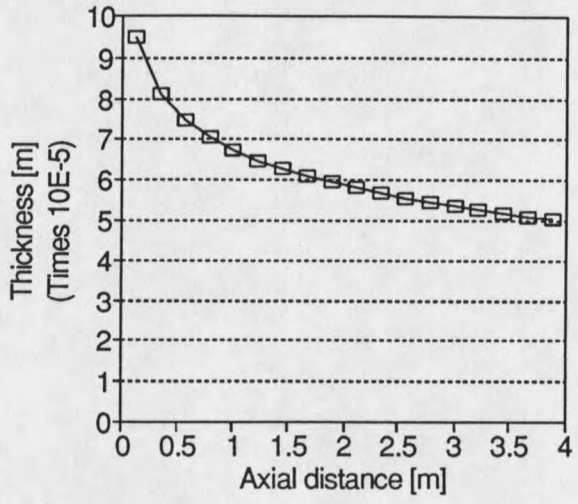

Figure 15: L_f as a function of axial distance, at t = 1day

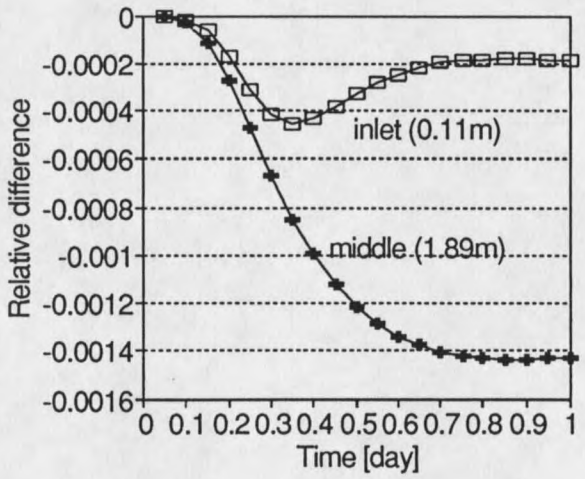

Figure 16: Differences in L_f as a function of time (inlet and middle)

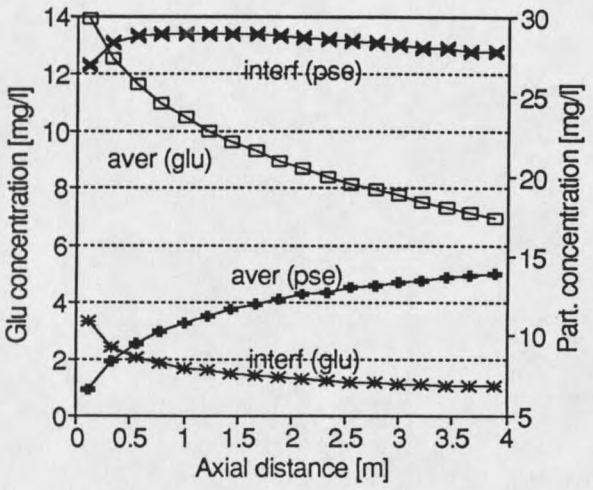

Figure 17: Average and interface concentrations versus axial distance

this difference (0.04%) is much less than the relative difference between the outlet thicknesses (0.14%). An explanation for this larger difference lies in the method of grid movement. Present implementation of the model uses a slightly different approach to update the grid than is described in the previous section. Instead of moving the first (inlet) surface horizontally, the last (outlet) surface is kept horizontal. The reason for this is that (a) the grid is updated only once per time step, thus there is no need to update the front of the grid before the rest is updated; (b) as Figures 6 and 15 show, the gradient of the thickness is less towards the outlet, than the inlet. Thus, the outlet interface of the shorter pipe was kept horizontal, while in the longer pipe this interface is in the middle, and thus tilted. This change of geometry changes the effective areas of the grid surfaces, so the solid velocity (u_s) and detachment changes, as well.

The average and interface concentration of *glu* and *pse* can be observed on Figure 17. These concentration values are shown as the function of axial distance at 1 day. As expected, both the average and interface concentration of *glu* decreases as the distance from the inlet increases. The shape of the average *pse* curve is also as expected. On the other hand, the interface concentration of *pse* is unexpected. There is a slight increase near the inlet of the pipe, and then the concentration slightly, but continuously drops to the end of the pipe.

To explain this, one has to examine what really happens near the interface. Let us consider a volume element at the interface in the bulk. There is a flux of *pse* into the volume element from the film, which is a function of the thickness. Diffusion transfers some to the next volume element, and some (insignificant) is produced by the biochemical reaction. The last process to consider is advection in the axial direction. Since the flow is laminar, near the interface the velocity of the liquid is very low. So, at the inlet there is no "incoming" *pse* through advection, but some (little) is moved to the next axial section. In the next section detachment is somewhat less, since the film is less thick, but the sum of the advected and detached *pse* exceeds the amount detached in the previous section. After a certain distance, however, the detachment becomes much less, thus the sum of advected and detached *pse* is less than the amount in the previous section. This explains the initial increase and then decrease in concentration near the interface. Related to this issue, but not significant

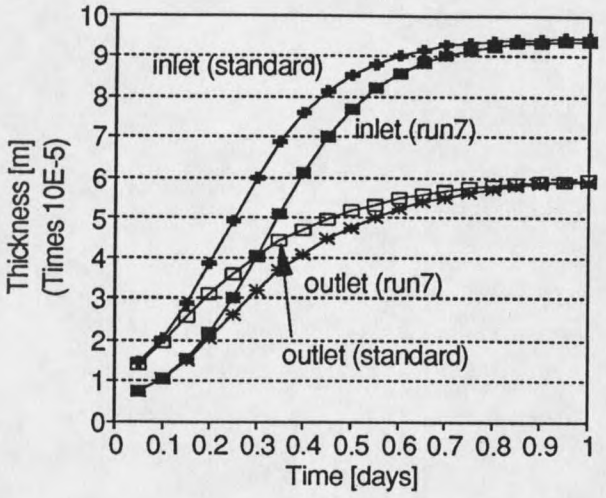

Figure 18: L_f as a function of time (standard and run7)

in the presented case, is the fact that axial advection is near 0 at the interface. This means that the residence time of particulates (here *pse*) is much greater than would be expected from the average velocity. Thus, if the concentration of particulates is large (comparable to the film), then this layer of liquid can act as a biofilm.

Effect of Initial Thickness

Figure 18 shows the result of run7, where the initial thickness of the film was changed from 10μ to 5μ. The inlet and outlet thickness values as functions of time are shown for both the standard run and run7. As expected, run7 reaches the same steady state thickness values, but the the time evolution lags behind that of the standard run.

Time Complexity

In order to determine the time complexity, a sketch of the algorithm is useful:

```
begin
  initialize system
  t = t_0
  while t < t_end
  begin
    calculate velocities
    calculate grid velocity
    move grid
    for all axial positions
    begin
      while not converge
      begin
        calculate Jacobians
        calculate fluxes
        build tridiagonal matrix
        solve system (Block-Thomas)
        update solution
        check convergence
```

end

end

$t = t + \Delta t$

end

end

The size of the system is determined by the following parameters: number of components ($c = N_{part} + N_{sub}$), number of reactions ($r = N_{rxn}$) total number of radial grids ($n = N_{rad} + N_{film}$), number of axial grids ($m = N_{axial}$), number of iterations (N_{iter}) and number of time steps to be performed ($N_{step} = (t_{end} - t_0)/\Delta t$). For simplicity a constant time step is assumed. Since there are $(n-1)(m-1) = O(nm)$ volumes, calculating velocities takes $O(nm)$ time. The same time ($O(nm)$) is needed to calculate the grid velocities, since $O(m)$ time is needed to calculate the interface velocities, and $(m-1)(n-2) = O(nm)$ faces have to be moved. At every axial section there are $O(n)$ surfaces, and for each surface 4 (two viscous and two inviscid) Jacobians of dimensions $c \times c$ are calculated, the time requirement is $4O(n)c^2 = O(nc^2)$. The same is true for fluxes, with the exception that instead of c^2 only c entries exist, thus it takes $O(nc)$ time only. To calculate the reaction terms $\mathbf{W}$, $O(nr^2c)$ operations are needed (see eq. 11). To calculate the source term Jacobian, $O(nr^2c^3)$ operations are necessary. In order to solve the block-tridiagonal

system $O(nc^3)$ operations are required [8]. This is a huge improvement on $O((nc)^3)$ complexity required if full Gauss elimination is used. Thus the overall complexity reads:

$$T = O\left(N_{step}\left[O(nm) + (m-1)N_{iter}\left(O(nc^2) + O(nr^2c^3) + O(nc) + O(nc^3)\right)\right]\right) \tag{78}$$

which reduces to

$$T = O(N_{step}N_{iter}mnr^2c^3). \tag{79}$$

In words, the complexity is a linear function of the grid size and time step size, quadratic in the number of reactions, and cubic in the number of components.

Parallelization Issues

Typical systems usually have 2 to 5 components, but could have hundreds or thousands of radial and axial grids. This might be essential for pipes of length in the range of kilometers. While the number of components in the model is determined by the system to be simulated, the granularity of the grid is in the hands of the user. However, large m and n values can significantly increase the required solution time.

An obvious possibility to reduce the time complexity is to use m processors, each solving a separate axial section. Since the equations are decoupled in the axial direction, and the equations have the same structure, an SIMD machine with m processors

could perform the same task in

$$T = O(N_{step} N_{iter} n r^2 c^3) \tag{80}$$

time.

A more complicated solution could use mn processors. Since at every axial section there is a block-tridiagonal matrix with n blocks, instead of using an inherently sequential, recursive method, an iterative method could be used to solve the tridiagonal system [9]. If k iterations are required for convergence, then the time complexity becomes

$$T = O(N_{step} N_{iter} k r^2 c^3). \tag{81}$$

It is hoped that $k \ll n$. A further complication with this approach is that the domain is not homogeneous in the radial direction: (1) The number of variables is less in the film compartment, (2) at the film/bulk interface and at the wall boundary conditions have to be handled. These complications make this method less suitable for massively parallel SIMD computers. Another possible method to solve tridiagonal systems is given in [13]

Other methods, that use different solving techniques could also be used, e.g. domain decomposition.

For further discussion on parallelization issues, see [13] and [14].

CHAPTER 6

CONCLUSIONS AND FURTHER WORK

This thesis gave an overview on biofilm systems, and issues involved in biofilm accumulation modeling. The focus was on biofilm systems in a given geometry, cylindrical pipelines. A mathematical formulation of components and processes were derived. The major processes included in the model are diffusion, advection, bio-chemical reactions, interfacial transfer processes. Based on these processes the governing equations were derived based on the conservation of mass principle. The resulting equations are coupled, nonlinear, partial differential equations.

A numerical method based on the finite volume approach was developed. An advantage of the method is that it allows change in the grid as the system evolves in time. To correctly solve the discretized equations in this moving grid environment the *Geometric Conservation Law* had to be used.

Finally, several examples were analyzed to determine the numerical behavior of the developed algorithm. These examples showed that the model produces acceptable results, and pointed out some interesting, unexpected phenomena.

In the future several tasks should or could be performed to improve the performance of the numerical method. The simplest improvements are to include variable time

steps and more sophisticated convergence checks. The model could be extended to include axial diffusion, as well. This would mean that the nonlinear solver should include the entire pipe, rather than a single section only. Of less importance is to extend the two dimensional (axisymmetric) geometry to three dimensions.

The algorithm to move the grid could be improved to avoid "jaggedness" mentioned earlier. For example, a better method could determine the first vertex velocity as the function of *all* centroid velocities, to minimize a certain parameter of the resulting grid (e.g. "jaggedness").

Further research has to evaluate the model against real-world data. Extensive work will be required to determine how the model performs in different geometries, flow regimes, and biological-chemical environments. Other research efforts should focus on determining the most important (sensitive) parameters. Finally, but not last, the model has to be updated regularly to include new knowledge and insight obtained about processes already modeled, or include newly found ones.

REFERENCES CITED

[1] Notter, R.H. and C.A. Sleicher: The eddy diffusivity in the turbulent boundary layer near a wall. *Chemical Engineering Science*, Vol. 26, pp. 161-171, 1971.

[2] Kirkpatrick, J.P. et al.: Mass and heat transfer in a circular tube with biofouling. *Water Research* Vol. 14, pp. 117-127, 1980.

[3] Characklis, W.G. and K.C. Marshall (editors) *Biofilms.* John Wiley & Sons, Inc., New York, 1990.

[4] Characklis, W.G. et al.: Modeling of biofilm systems. IAWPRC Scientific and Technical Report, May 1989.

[5] Characklis, W.G. R. Bakke and M.H. Turakhia: Theoretical and experimental analysis of a *Pseudomonas Aeruginosa* biofilm. *Wat. Sci. Tech.*, Vol. 20, No. 11/12, pp. 45-51, 1988

[6] Thomas, P.D. and C.K. Lombard: Geometric conservation law and its application to flow computations on moving grids. *AIAA Journal*, Vol. 17, No. 10, pp. 1030-1037, 1979.

[7] Grossman, B. and R.W. Walters: Analysis of flux-split algorithms for Euler's equations with real gases. *AIAA Journal*, Vol. 27, No. 5, pp. 524-531, 1989.

[8] Fletcher, C.A.J.: *Computational Techniques for Fluid Dynamics*, Springer-Verlag, New York, 1988.

[9] Boghosian, B.M.: Data parallel computation on the CM-2 Connection Machine computer. II. Basic linear algebra algorithms. Technical Report, DP89-3, Thinking Machines Corporation, October 1989.

[10] Wanner, O. and W. Gujer: A multispecies biofilm model. *Biotechnology and Bioengineering*, Vol. 28, pp. 314-328, 1986.

[11] Janus, J.M.: Advanced 3-D CFD algorithm for turbomachinery. Ph.D. dissertation, Mississippi State University, 1989.

[12] Van Leer, et al.: A comparison of numerical flux formulas for the Euler and Navier-Stokes equations. AIAA paper, No. 87-1104-CP, 1987.

[13] Codenotti, B. and M. Leoncini: *Parallel Complexity of Linear System Solution*, World Scientific, Singapore, 1991.

[14] Akl, S.G.: *The Design and Analysis of Parallel Algorithms*, Prentice-Hall Inc., Englewood Cliffs, 1989.

MONTANA STATE UNIVERSITY LIBRARIES
3 1762 10192399 1

HOUCHEN
BINDERY LTD
UTICA/OMAHA
NE.